Cement and Concrete Research 40 (2010) 914–923

Contents lists available at ScienceDirect

Cement and Concrete Research

journal homepage: http://ees.elsevier.com/CEMCON/default.asp

Rapid evaluation of alkali–silica reactivity of aggregates using a nonlinear resonance spectroscopy technique

Jun Chen [a], Amal R. Jayapalan [a], Jin-Yeon Kim [a], Kimberly E. Kurtis [a,*], Laurence J. Jacobs [a,b]

[a] School of Civil and Environmental Engineering, Georgia Institute of Technology, Atlanta, GA, 30332, USA
[b] GWW School of Mechanical Engineering, Georgia Institute of Technology, Atlanta, GA, 30332, USA

ARTICLE INFO

Article history:
Received 21 August 2009
Accepted 6 January 2010

Keywords:
Alkali–aggregate reaction (C)
Nonlinear acoustics
Crack detection (B)
Microcracking (B)
Mortar (E)

ABSTRACT

A new nonlinear acoustic technique — Nonlinear Impact Resonance Acoustic Spectroscopy (NIRAS) — is developed and used to characterize the alkali-reactivity of different aggregates. Cementitious materials such as mortar and concrete exhibit a hysteretic and nonlinear elastic behavior in their constitutive relations. This hysteretic nonlinearity is associated with interfacial debonding between the different constituents, and it changes with the progress of damage such as that induced by the alkali–silica reaction (ASR). One of the consequences of the hysteretic nonlinear property of these materials is the decrease in resonance frequencies, with increased excitation amplitude. This shift in the resonance frequency as a function of the material nonlinearity parameter can be used to directly characterize the damage state of the material. This research tracks the variation of the nonlinearity parameter during a standard accelerated mortar bar test (AMBT) to assess the potential for alkali-reactivity of aggregates. The results show that the NIRAS technique is more sensitive than conventional linear acoustic methods and is capable of accurately characterizing the reactivity of the aggregates examined. Furthermore, the results show advantages over standard expansion measurements for differentiating various aggregates having similar levels of reactivity, particularly at early test ages. These changes in the nonlinearity parameter are benchmarked against results from a petrographic analysis. Thus, the proposed NIRAS is a promising technique for the rapid identification of alkali-reactive aggregates.

1. Introduction

Alkali–silica reaction (ASR) is generally considered as a complex chemical process occurring in cement-based materials, where the hydroxyl ions in the highly alkaline pore solution attack the siloxane groups (Si–O–Si) of siliceous mineral components of aggregates. Aggregates containing siliceous minerals which are disordered, amorphous, strained, or cryptocrystalline are known to be particularly susceptible to this reaction [1–3]. Hydroxyl ions together with alkali metal cations (sodium or potassium) bind with siliceous species derived from the reactive minerals to form a cross-linked alkali–silica gel. The alkali–silica gel swells with imbibition of moisture from the surrounding material [4]. The expansion of gel results in cracking when the swelling stress exceeds the tensile capacity of the paste or aggregates. As expansion increases, cracks grow and eventually coalesce; the strength and modulus of the material are decreased and the permeability is increased [5].

Currently, the reactivity of aggregates is most commonly determined by expansion measurement methods and petrographic analyses [6,7]. Expansion measurement methods such as accelerated mortar bar tests (AMBT) [8,9] and concrete prism tests (CPT) [10] are the most widely used methods currently in practice. However, AMBT has been criticized as an overly severe method, while the one year test duration of CPT reduces its usefulness for rapid identification of varying or marginal sources [7,11]. Petrographic methods [12] are usually used as supplementary, rather than independent, techniques to assess the potential for reactivity [13]. For example, Ben Haha et al. [14] used image analysis techniques applied to scanning electron micrographs to characterize the "degree of reaction", correlating the changes in the microstructure with expansion measurements.

Lately, researchers have been working to develop new test methods by trying to balance the tradeoffs between reliability and test duration [15–18]. Nevertheless, nearly all of these new methods are still based on the principle of length measurement, and the modifications are focused on the experimental details, such as the size of the aggregates, size of the samples or the storage temperature. Meanwhile, practical and routine use of these new methods remains on the horizon, with concerns regarding the suitability of some of these proposed methods [18].

Expansion methods measure the length change of samples due to ASR. However, ASR damage in concrete not only leads to macroscopic changes such as the increased length of unrestrained samples, but also alters the material properties at the microscopic scale. For instance, experiments showed that the elastic modulus of alkali–silica gel was

* Corresponding author. Tel.: +1 404 385 0825.
E-mail address: kkurtis@ce.gatech.edu (K.E. Kurtis).

0008-8846/$ – see front matter © 2010 Elsevier Ltd. All rights reserved.
doi:10.1016/j.cemconres.2010.01.003

significantly different from that of cement paste or aggregates, and that it varied under different internal pressures [19]. From the point of view of micromechanics, the occurrence of ASR gel and microcracking throughout the progression of ASR damage must increase the heterogeneity of multiple-phase cement-based materials, and change the overall elastic properties of this composite material. Thus methods measuring the changed microstructural material properties during ASR have drawn increasing interest recently. A few experimental studies have attempted to correlate the variation of material properties including Young's modulus, and tensile and compressive strength of ASR-affected concrete prisms with the development of damage [20–22]. In addition, several recent works also employed conventional nondestructive evaluation (NDE) techniques to assess ASR damage in concrete prism samples. These conventional NDE techniques included the measurement of wave speed and/or linear attenuation [23–25], which were essentially correlated to the change of elastic properties.

Although these techniques provide a perspective for the ASR characterization that is different from the conventional approach of expansion measurement, a fundamental assumption of linear elastic constitutive material behavior is adopted in these elastic modulus or linear acoustic measurements. It is thus assumed that the elastic properties of these materials are independent of the elastic deformation. However, both mortar and concrete do not follow this assumption. The sensitivity and reliability of these techniques based on linear measurements are thus likely not appropriate for use as a standard laboratory method for screening aggregates.

Previous research [26,27] has consistently demonstrated a hysteretic nonlinear elastic behavior in mortars and concretes, and has shown that any damage to the microstructure results not only in changes of linear parameters, such as a decrease in Young's modulus and an increase in the attenuation coefficient, but also increases the nonlinearity parameters. The nonlinearity parameters are more sensitive to the progress of damage when compared to their linear counterparts [28]. This is particularly important for cement-based materials, because their inherent heterogeneity may affect the measurements by the introduction of unexpected deviations. Therefore, the relatively low sensitivity of linear measurements is most likely due to their false assumption of linear elasticity, and these linear measurements are not as well-suited to quantitatively characterize the nonlinear progression of damage in cement-based materials.

In recent years, experimental techniques [28–32] based on nonlinear acoustic measurements have attracted significant attention for their potential application to early diagnosis of material damage. For example, with the development of small-scale damage (e.g., microcracking) due to fatigue, the stress–strain relationship of the material deviates from its initial linear behavior and the nonlinear contribution increases [28–30]. The nonlinearity of the constitutive relation essentially provides the theoretical background for various nonlinear acoustic phenomena observed in elastic waves propagating in damaged materials. For instance, Kim et al. [28], Herrmann et al. [29] and Pruell et al. [30] reported the generation of a second order harmonic of the incident wave and related this phenomenon to the fatigue damage in metallic and alloy materials. Kögl et al. [31] also numerically simulated the generation of higher harmonics for the detection of cracks in flat slabs. Donskoy et al. [32] and Ekimov et al. [33] investigated cracks in steel samples using the phenomenon of nonlinear cross-interaction between a low frequency vibration and high frequency elastic waves (nonlinear wave modulation).

Given the recent advances in the application of nonlinear acoustic techniques in metallic materials, there is growing interest in using these techniques to characterize damage in cement-based materials. Warnemuende and Wu [34] applied a nonlinear modulation method to differentiate between various degrees of damage in mortar cylinders subjected to different loading conditions. Payan et al. [35] observed a shift of resonance frequencies in thermally damaged concrete samples. Chen et al. [36] provided preliminary measurements of ASR damage with a nonlinear modulation technique. These results suggest the potential of nonlinear acoustic techniques for damage characterization in cementitious materials.

This research proposes a novel nonlinear acoustic technique termed "Nonlinear Impact Resonance Acoustic Spectroscopy" (NIRAS) to assess progressive damage occurring in mortar bars undergoing alkali–silica reaction under a standard accelerated exposure condition. The principle of NIRAS is based on a shift of the resonance frequency of the sample due to the increasing material nonlinearity, such as with progressive ASR damage. A nonlinearity parameter that represents a measure of ASR damage present in a sample is used to track the accumulation of damage in the sample with increasing duration of exposure to standard accelerated test conditions. Here, aggregates with varying alkali-reactivity are characterized by the NIRAS method during standard accelerated testing conditions. In addition, standard expansion tests and linear elastic modulus measurements are simultaneously conducted, and the results from these three different approaches are compared and correlated to one another. It is found that the NIRAS technique is much more sensitive than linear acoustic measurements for differentiating ASR-damaged samples from those ASR intact samples. The NIRAS technique is also able to accurately distinguish among aggregates of varying reactivity at a relatively early age, when compared to the standard expansion-based test methods. Through an analysis of the accompanying petrographic images, the NIRAS results may be linked to the different stages of ASR microstructure change, such as gel formation and progressive cracking.

2. Experiment

2.1. Sample preparation

Four fine aggregates, all from U.S. sources, were examined according to AASHTO T 303 [9]. The difference between the accelerated mortar bar tests, AASHTO T 303 and the commonly used ASTM C 1260, is only in the water-to-cement ratio, which are 0.50 and 0.47 respectively. The aggregates used for the tests were the following: (1) a highly reactive aggregate from Texas with an expansion of 0.456% at 14 days (after demolding), (2) a moderately reactive aggregate from Alabama with an expansion of 0.136% at 14 days, (3) a marginally reactive aggregate from Georgia with an expansion of 0.098% at 14 days, and (4) a non-reactive dolomitic aggregate from Georgia with an expansion of 0.069% at 14 days. The terminology used here to describe the reactivity of aggregates will be discussed in Section 3.3.1 that discusses the expansion test results. The mineralogical analysis reveals that the reactive component of aggregates #1 and #2 is chert and the reactive component of aggregate #3 is strained quartz. For each aggregate, eight mortar samples of dimensions $285\times25\times25$ mm ($11^1/_4\times1\times1$ in.) were cast according to standard procedures [8,9], three of which were used for expansion measurements, three for NIRAS tests, one for compression testing to obtain elastic modulus values, and one for microscopy. A Type I cement (of potential Bogue composition 46.11% C_3S, 22.93% C_2S, 8.52% C_3A and 9.59% C_4AF and 0.83% Na_2O_{eq}) was used for preparing the samples and the mixing procedure was in compliance with AASHTO T 303 [9].

The samples were cured at ~100% relative humidity and 23 °C (73.4 °F) for 24 h. After demolding they were immersed in tap water and placed in an oven at 80 °C (176 °F) for another 24 h. The first set of expansion measurements, compression tests and acoustic experiments was then conducted to obtain the initial results at the end of the curing period. To induce ASR damage, mortar bars were then immersed in a 1 N NaOH solution at 80 °C (176 °F), according to AASTHO T 303. Samples were then taken out of the solution at regular intervals for expansion measurements, compression testing, NIRAS testing, and microscopic analysis.

2.2. Expansion tests

The expansion measurements were conducted according to AASHTO T 303, but with an additional, but minimal, "out-of-exposure time" necessary for the measurement of the elastic modulus and NIRAS testing. Since the time required to perform the elastic modulus and NIRAS measurements is currently 15 min, mortar bars remained at ambient conditions during that time period. In addition, to minimize sample variability during the assessment of both modulus and NIRAS measurements, all samples were conditioned in an environmental chamber at 50% relative humidity and 23 °C (73.4 °F) for 30 min after their removal from the high temperature, high alkaline environment used in AASHTO T 303. The effect of this additional 45 min of "out-of-exposure time" on expansion has been previously assessed for these aggregates and was found to be negligible [37].

2.3. Compression tests

The elastic moduli of mortars were calculated based on the stress–strain measurements made during compression experiments performed over the 14-day accelerated exposure period. For each aggregate, a 88.9-mm (3.5-in.) long specimen was cut from one mortar bar when the specimens were taken from the water after the 24-hour curing period. The stress–strain behavior of the specimens under compressive loading was recorded using a 100-kN universal testing machine, and an extensometer (with a 0.004 strain accuracy) affixed on the specimen's surface. The specimens were loaded up to 40% of the initial compressive strength, which was measured right after the curing in water. Five measurements were made for each specimen at each age to minimize the variability in the tests, and the average of the calculated modulus at each age was used for comparison with expansion and NIRAS data.

2.4. NIRAS measurements

2.4.1. Experimental procedure

In the NIRAS tests, mortar bar samples were cut to a length of 254 mm (10 in.). The samples were then fixed at one end (embedded length was 25.4 mm (1 in.)) using a clamping device and free at the other end (so that it was a beam with a fixed-free boundary condition). The cantilever length of the beam was 228.6 mm (9 in.), and its thickness was 25.4 mm (1 in.). An accelerometer was affixed to one surface near the free end, and the impact energy was applied in the middle of the opposite surface with an instrumented hammer. The impact signal and received vibration signal were captured and recorded by a digital oscilloscope. A schematic diagram of the experimental setup is shown in Fig. 1.

2.4.2. Underlying analytical background

As previously described, the shift of the resonance frequency as measured by the NIRAS technique essentially arises from the material nonlinearity. For brittle inhomogeneous materials such as rock and concrete, in addition to the inherent nonlinearity, the hysteresis in the stress–strain relationship also contributes to the total nonlinearity of the materials [27,38]. Guyer and McCall proposed a phenomenological model for this hysteresis effect [39]. According to this model and the classical nonlinear constitutive relation [40], the elastic modulus of a material having nonlinear hysteretic effects E can be assumed as

$$E = E_0\left[1 + \beta\varepsilon + \delta\varepsilon^2 + \alpha(\Delta\varepsilon + \varepsilon \cdot \mathrm{sgn}(\dot{\varepsilon}))\right] \quad (1)$$

where E_0 is the linear elastic modulus, β and δ are the coefficients of cubic and quartic anharmonicities, $\Delta\varepsilon$ is the strain amplitude, ε and $\dot{\varepsilon}$ are the strain and strain rate, α is the measure of hysteresis, and sgn is the sign function.

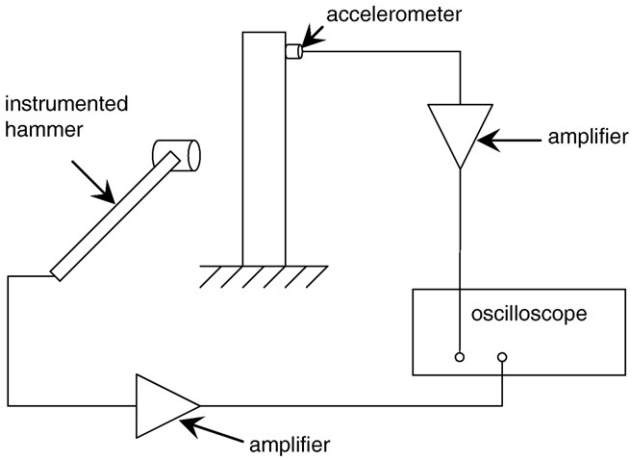

Fig. 1. Schematic plot of experiment setup.

For samples made of a linear elastic material, the linear resonance frequencies remain constant and can be determined by material properties, sample geometry and boundary conditions [41]. In contrast, the resonance frequencies of samples made of a material that follows Eq. (1) change with the amplitude of excitation energy, and are called nonlinear resonance frequencies. An approximate expression for the nonlinear resonance frequencies f can be derived in a similar way to [42] for the resonance of longitudinal vibrations, as below,

$$\frac{f_0 - f}{f_0} \approx \lambda_1 \cdot \Delta\varepsilon + \lambda_2 \cdot \Delta\varepsilon^2 \quad (2)$$

where f_0 is the linear resonance frequencies corresponding to the linear elastic modulus E_0, λ_1 and λ_2 are the nonlinear constants proportional to α and δ, respectively.

For nonlinear materials, like concrete and mortar, it has experimentally been observed that the linear term of the right-hand side of Eq. (2) which is related to the hysteresis constant λ_1 is dominant when the excitation is relatively low [27]. The shift of resonance frequency thus varies quasi-linearly with the increase in excitation amplitude. As the excitation amplitude grows, the quadratic term in Eq. (2) cannot be neglected. In the experiments presented in this paper, only the linear term of Eq. (2) is considered since the impact excitation applied is not very strong. Discussions about these concepts are given elsewhere [42].

In previous research using the nonlinear resonance methods [27,38], the resonance modes of the samples were excited by sweeping through a wide frequency range around the specific resonance mode of interest. Therefore, in such experiments, the value of resonance modes has to be known a priori in order to determine the appropriate frequency sweeping range. In contrast, for the proposed NIRAS technique, the resonance modes of mortar samples are generated simply by an impact excitation with an instrumented hammer, and an initial estimate is not needed. This is an advantage, particularly since the resonance mode may change due to increasing damage in the sample with increasing exposure, such as the ASR deterioration in this research. Another advantage of the NIRAS technique is that multiple resonance modes can be obtained from the same signal generated by a single impact. NIRAS is more efficient than other techniques using continuous sine waves as excitation sources, in which different transducers with different center frequencies are needed to excite multiple resonance modes.

2.5. Microscopy

The samples for the microscopy were cut to a length of 12.7 mm (0.5 in.) with a low speed saw using ethanol as a lubricant after the

initial curing of the sample in water at 80 °C. The cut specimens were then polished to 600-grit size using a grinder/polisher.

Prior to imaging, the samples were gently wiped with a damp cloth. When necessary, the imaging surface was polished for ~30 s. Digital images (1600 by 1200 pixels) of the surfaces were taken at different locations on each specimen using a stereo-microscope (Leica MZ6) at magnifications of 40× and 80×.

Imaging was carried out at the same specimen locations using an indexible stage, allowing characterization of ASR damage over the exposure period. Thus, the extent of the formation of alkali–silica gel, aggregate/paste debonding, aggregate degradation, crack initiation and crack propagation at the same location was studied through the repeated imaging.

3. Experimental results and discussions

The linearity of the NIRAS experimental setup is first validated to quantify the instrument nonlinearity for the system proposed to make these NIRAS measurements. The sensitivity of the NIRAS technique for differentiating the ASR-damaged samples from the undamaged control samples is then shown through a comparison with results from a conventional resonance vibration. Finally, the NIRAS technique is applied to distinguish between four different aggregates of varying alkali–silica reactivity, and the results are analyzed and correlated to the accompanying expansion data and linear elastic modulus measurements.

3.1. Linearity of NIRAS experimental setup

In general, there are a number of sources of nonlinearity inherent in the experimental setup, and these nonlinearities can be coupled with the material nonlinearity that is proposed to be measured. For example, since samples are fixed by a clamping device, the contacting surfaces (between the sample and the fixture) can produce a strong nonlinearity if not properly considered. In addition, all electronic devices and cables can produce spurious electrical nonlinearity. Therefore, it is important, at the beginning of the experiment, to confirm the linearity of the measurement system as a whole to ensure that only the nonlinearity of the mortar samples, and not the instrumentation nonlinearity, is being measured.

A polymethyl methacrylate (PMMA) slender bar, of approximately the same dimension as the mortar samples, was used in the system linearity test, assuming that the PMMA is linear at the same level of displacement (or excitation). A shift of resonance frequency of the PMMA bar will appear if any nonlinearity exists in the experimental setup or electronic devices. Twenty vibration signals for varying impact energies were acquired. A representative time-domain vibration signal from the PMMA bar is shown in Fig. 2. The frequency spectra of these signals were obtained with the fast Fourier transform (FFT), and the spectra around the first resonance mode are shown in Fig. 3. It is seen that the resonance frequency at different impact energies remains unchanged. This demonstrates that the total nonlinearity from the mechanical fixture and electronic devices is negligibly small, and thus the measured nonlinearity for mortar bars presented later in this paper is only due to the material, plus any damage to the material.

3.2. Sensitivity of NIRAS to ASR-induced damage

The sensitivity of NIRAS to ASR-induced damage is examined by comparing measurements made on an ASR damaged, and an undamaged mortar bar. These results are then compared with the results from a conventional linear resonance vibration technique.

Two mortar samples were cast with aggregate #1 which is known to be highly reactive by AASHTO expansion tests. Both were proportioned and cured per AASHTO T 303, and while one was stored

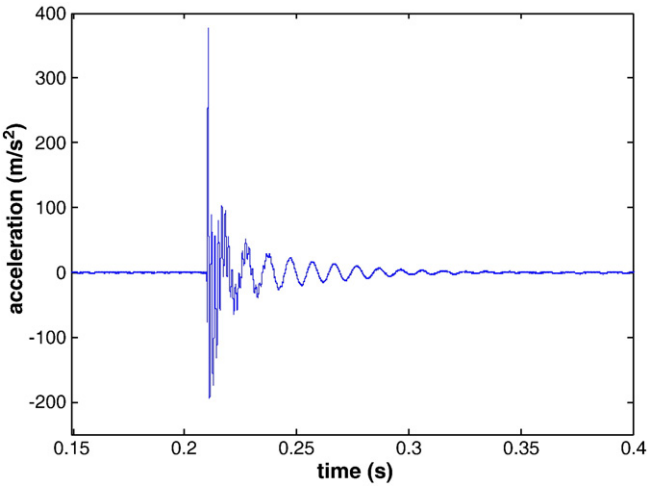

Fig. 2. A typical vibration signal in time domain.

in 80 °C (176 °F) 1 N NaOH solution to induce ASR damage, the other was immersed in tap water at 80 °C (176 °F) as a control specimen. Again in each test, twenty impacts were imparted to each bar with different energies, and the experiment was repeated at various intervals with the increasing exposure period. Fig. 4 shows a comparison of the resonance frequencies for the control sample and damaged sample after 4 days of exposure. It is seen in Fig. 4a, for the control sample, that there is a minor decrease of the resonance frequency over the increased excitation; this may be caused by the intrinsic nonlinearity of the mortar. In contrast, the shift of resonance frequency in the damaged sample is much more pronounced as shown in Fig. 4b. It is proposed that this observed shift in resonance frequency is due to the development of ASR damage.

As can be theoretically predicted, it is also observed in Fig. 4 that the resonance frequency remains constant if the excitation is limited to values below a certain level (that is, when $\Delta\varepsilon$ in Eq. (2) is very small). Therefore, the resonance frequency at the smallest excitation in Fig. 4 may be taken approximately as the linear resonance f_0 of the sample. As a measure of nonlinearity, nonlinearity parameters can be defined as in Eq. (2) through a relationship between the shift of the resonance frequency $\Delta f = (f_0 - f)$ normalized by the above-defined linear resonance frequency f_0 and the strain amplitude $\Delta\varepsilon$. In addition, it is known from Eq. (2) that when the excitation is low, the quadratic term is negligible and the shift of resonance frequency is proportional to the excitation, where the slope corresponds approximately to the

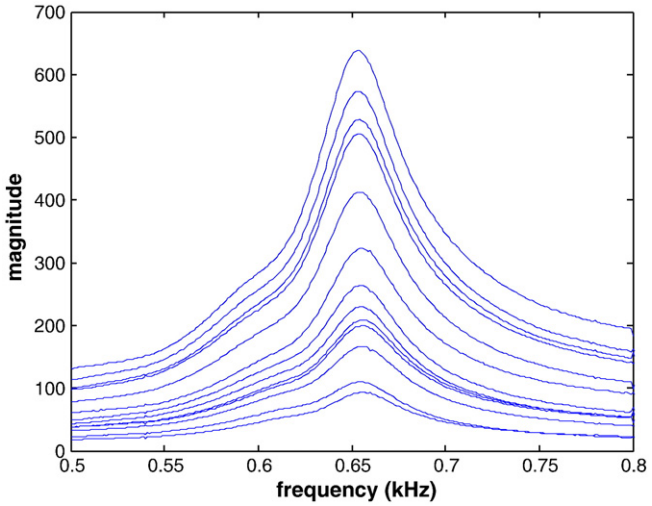

Fig. 3. Resonance of PMMA bar for different levels of impact energy.

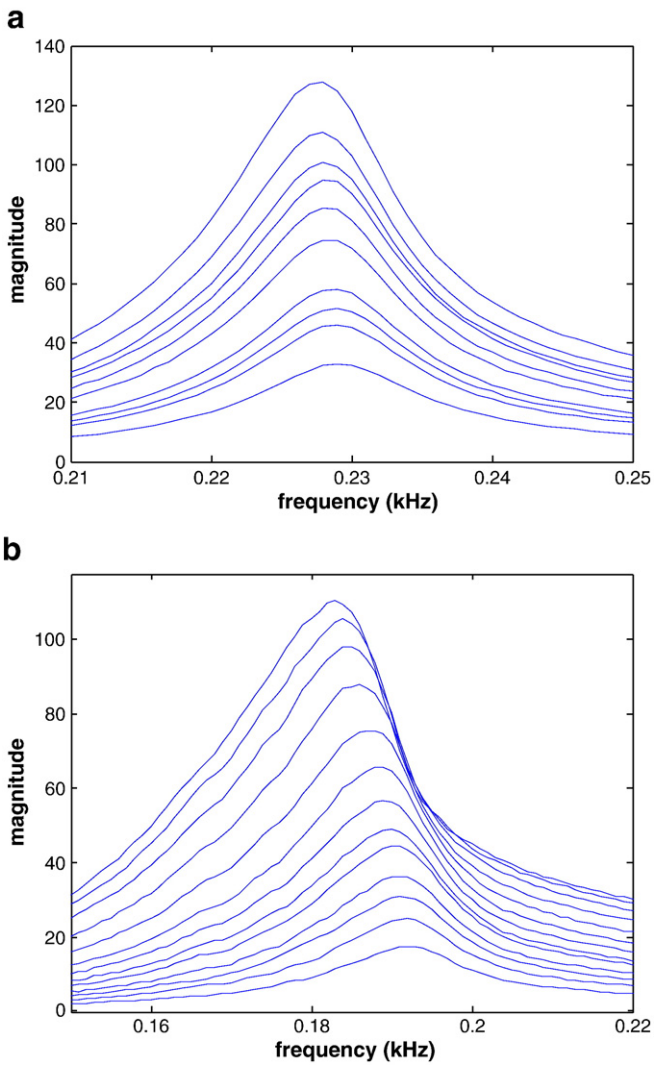

Fig. 4. (a) Resonance of intact mortar sample with increasing impact energy. (b) Resonance of damaged mortar sample with increasing impact energy.

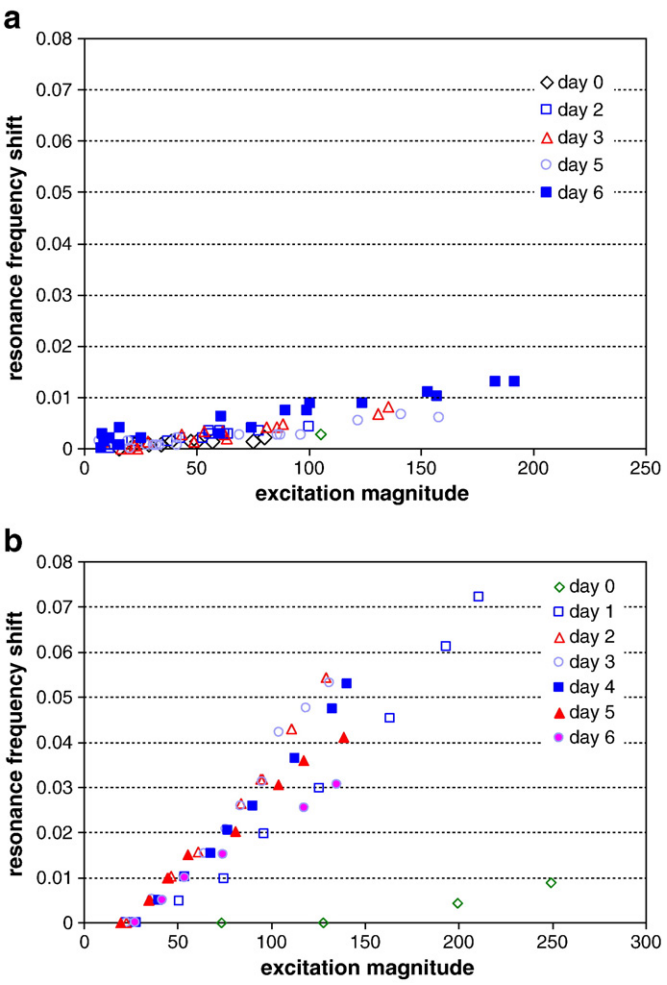

Fig. 5. (a) Resonance frequency shift versus excitation magnitude with increased exposure time for a control sample. (b) Resonance frequency shift versus excitation magnitude with increased exposure time for an ASR-damaged sample.

hysteresis constant λ_1, which is defined as the nonlinearity parameter used in this paper.

Fig. 5 presents the variation of the shifts of the resonance frequencies as a function of excitation magnitude up to 6 days of exposure time, for both the control and damaged samples. There is a clear linear relationship between the shift of the resonance frequency and the excitation magnitude for the ASR-damaged sample at every specific exposure time as shown in Fig. 5b. The slope of this relationship, i.e., the nonlinearity parameter (being close to the hysteresis constant, λ_1), has a visible change (increase or decrease) with the increasing exposure time and, thus, with increasing ASR-induced damage. In contrast, Fig. 5a shows that the shift of the resonance frequency has no obvious change versus excitation magnitude with an increase in exposure time. This indicates a satisfactory level of sensitivity for the increasing ASR damage in the mortar using the nonlinearity parameter obtained from this measurement.

Furthermore, the sensitivity of the NIRAS technique is compared to the conventional linear vibration method. As is well-known in classical vibration theory [41], the linear resonance frequency of a sample is determined by the linear elastic modulus of the material used, in addition to the geometry and the boundary conditions of the experimental specimen. The linear resonance frequency could thus be affected by the development of ASR damage because, as will be presented in Section 3.3.2, ASR does induce changes in the elastic modulus of the tested specimens. Therefore, the resonance frequency at the smallest excitation on each exposure day (practically considered as the linear resonance frequency as described above) is selected as the representative parameter of the conventional linear vibration method for a comparison with the NIRAS results. Both the linear parameter (linear resonance frequency) and the nonlinearity parameter of the NIRAS technique (i.e., the slope in Fig. 5) are normalized by their individual value before exposure (i.e., day 0) and are plotted in Fig. 6 up to six days of exposure time. It is observed in Fig. 6 that the normalized linear resonance has a maximum of 10% variation, while the normalized nonlinearity parameter has an increase as much as 10 times its initial normalized value. The comparison in Fig. 6 indicates that the proposed NIRAS technique is significantly more sensitive than the linear vibration method in quantifying ASR damage.

3.3. Differentiation of aggregates with varying reactivity

Four different aggregates with different alkali-reactivity were used to cast mortar samples for expansion testing, elastic modulus measurements and evaluation by the NIRAS technique. The results of these three different tests are discussed in this section.

3.3.1. Expansion measurement

The average expansions with standard deviation bars for three mortar samples cast with each aggregate over the 14-day exposure period are shown in Fig. 7. According to the guidance provided in

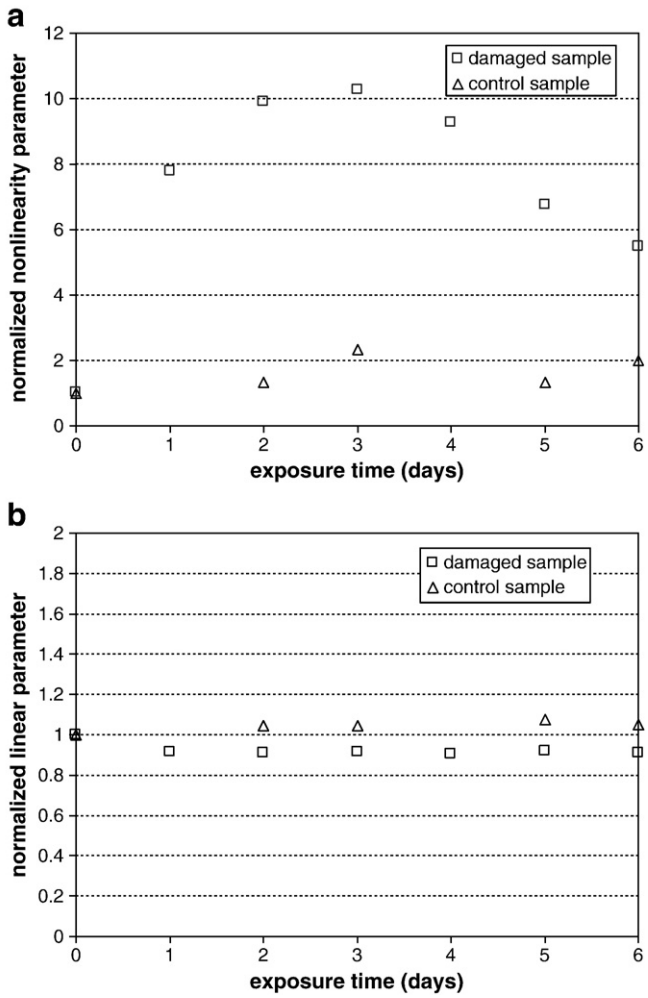

Fig. 6. (a) Sensitivity of NIRAS for differentiating ASR-damaged sample and control sample. (b) Sensitivity of linear resonance vibration method for differentiating ASR-damaged sample and control sample.

AASHTO T 303, aggregate #4 is considered innocuous since its expansion at 14 days from zero reading is less than 0.10%. Expansions at 14 days of exposure for aggregates #1, #2, #3 and #4 are 0.456%, 0.136%, 0.098% and 0.069%, respectively. It is also seen in Fig. 7 that the initial rate of expansion for aggregate #1 exceeds those for the other potentially reactive aggregates (#2 and #3). Also, the expansion data for aggregate #2 remain higher than those for aggregate #3 throughout the test period. Therefore, based upon the expansion results, in the following discussion, aggregates #1, #2 #3 and #4 will be termed "highly reactive," "moderately reactive," "marginally reactive" and "non-reactive" respectively.

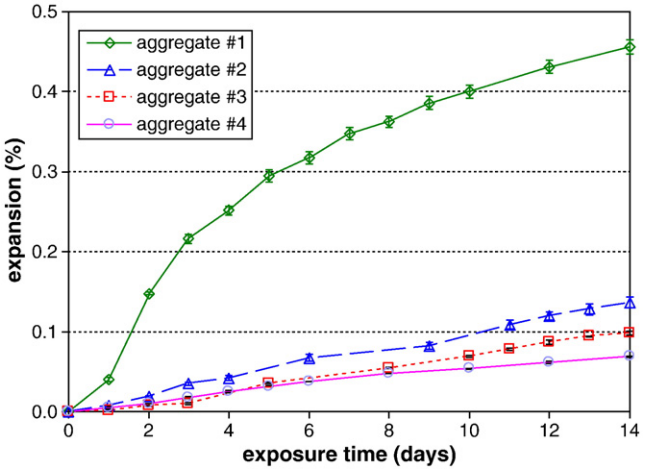

Fig. 7. Results of AASHTO T 303 expansion measurements.

3.3.2. Elastic modulus measurement

The variation of elastic modulus of mortar samples with respect to exposure time for these four aggregates is shown in Fig. 8 and the standard deviations for the modulus measurements are very small. It is seen in Fig. 8 that the modulus of mortars containing aggregates #1 and #4 is substantially different from those of aggregates #2 and #3 even before the exposure to aggressive solution (day 0). This variation at day 0 could be attributed to the differences in the aggregates themselves (e.g., elastic modulus) and their bond with the surrounding paste, which can be influenced by factors such as the aggregate surface texture, angularity, and maximum size as shown in Fig. 9. In general, the measured modulus of elasticity decreases with exposure time for the potentially reactive aggregates, and increases (presumably due to continued cement hydration) for the innocuous aggregate #4. The modulus of the highly reactive aggregate #1 is seen to decrease most rapidly during the first 4 days when compared to that of the other aggregates. These results are expected as the elastic modulus of cement-based materials is a property which is sensitive to defects, such as ASR-induced microcracking and debonding. However, the variations in elastic modulus between the moderately reactive aggregate #2 and marginally reactive aggregate #3 are indistinguishable from each other in the data in Fig. 8. Overall, although such tests might provide an indication of the influence of the ASR damage on the mechanical response in the cases of highly reactive or innocuous aggregates, these results suggest that mechanical measurements of elastic modulus are not suitable as a practical method for distinguishing among aggregate of moderate to marginal reactivity.

3.3.3. NIRAS measurements

After demonstrating that the proposed NIRAS technique can effectively differentiate the ASR-damaged sample from its intact counterpart (Fig. 5), the NIRAS measurements are used to determine if the NIRAS technique can be used to distinguish aggregates with varying alkali-reactivity. Fig. 10 shows the variation of normalized nonlinearity parameters of four aggregates over the 14-day exposure period, where the nonlinearity parameters were calculated in the same manner as in Fig. 5, i.e., the slope of the linear relationship between the shift of the resonance frequency and excitation magnitude. Similar to the elastic modulus, the initial values of nonlinearity parameters for these four aggregates before the exposure (day 0) were slightly different, and the normalization by the initial value on day 0 was enforced for the nonlinearity parameters at each

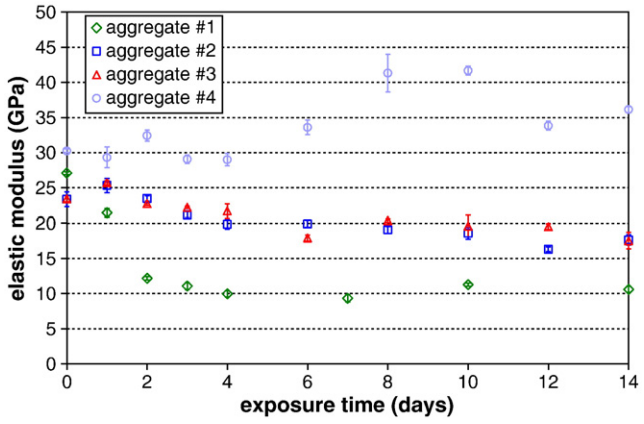

Fig. 8. Results of elastic modulus measurements.

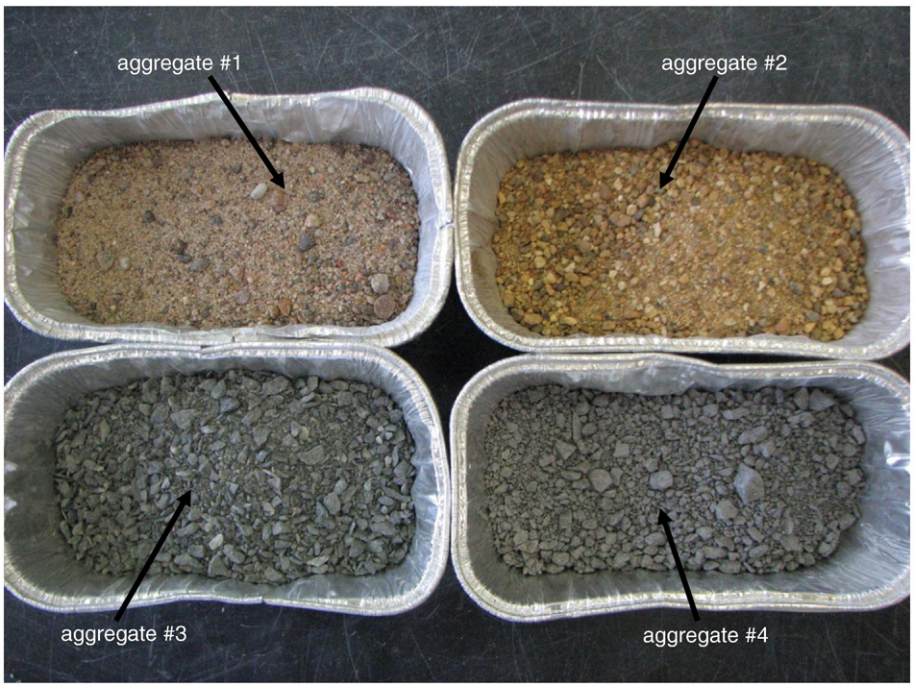

Fig. 9. Four different aggregates used (aggregates in this photograph are not graded).

exposure age to eliminate the effect of different intrinsic material nonlinearity. The average of the three specimens is used in Fig. 10 for all four aggregates and the standard deviation bar of aggregate #1 is also included.

First, the nonlinearity parameter of the innocuous aggregate #4 remains below a small value of 2, indicating that the material nonlinearity due to ASR throughout the exposure period did not significantly increase when compared to its initial value on day 0. The minor increase in nonlinearity parameter of aggregate #4 could be due to the heating-and-cooling cycle during tests or instrument nonlinearity. In contrast, the nonlinearity parameter of the highly reactive aggregate #1 increases rapidly during the initial 4 days of exposure, reaching nearly 10 and then decreases to a relatively stable value. The large difference of nonlinearity parameters between aggregates #1 and #4 indicates that the proposed NIRAS technique is sensitive to the ASR-induced damage of materials in these experiments, and not the other potential nonlinearity sources. The rapid increase in the nonlinearity parameter prior to day 4 for aggregate #1 indicates the relatively rapid rate of reaction and damage with this highly reactive aggregate which is consistent with the expansion measurements in Fig. 7, although the decrease of nonlinearity parameter after day 4 is not observed in expansion data. (The discussion of this phenomenon is provided later in this paper.) The highly reactive aggregate #1 and inert aggregate #4 can be considered to represent two relative extremes in behavior in this study, and their behavior observed by NIRAS is distinct at early test ages. Their behavior is distinct as well in the measurements of expansion and Young's modulus as shown in Figs. 7 and 8.

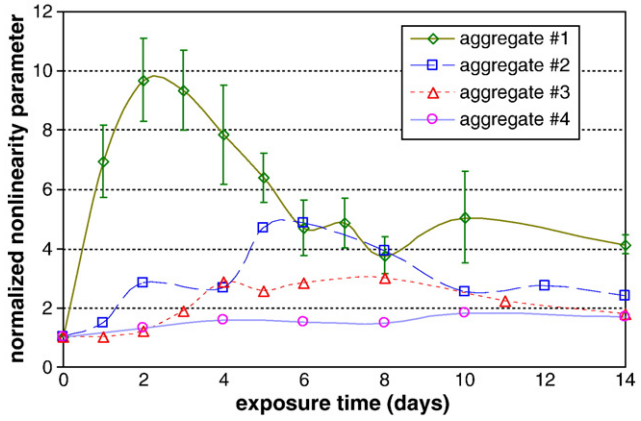

Fig. 10. Variation of normalized nonlinearity parameter with respect to exposure time (the lines connecting data points are only guides for the eye).

The trends in expansion (particularly at the early exposure times) and elastic modulus are not clearly distinct for aggregates #2, #3 and #4. The moduli of aggregates #2 and #3 are virtually indistinguishable over the test period. In the expansion tests, the greater potential reactivity of aggregate #2 is not clearly apparent until the end of the test. Moreover, the expansion of aggregate #3 was lower than that of aggregate #4 until about 5 days, even though aggregate #3 had a higher expansion at 14 days. In comparison, as shown in Fig. 10, the nonlinearity parameters of aggregates #2, #3 and #4 increased steadily, and by day 6, the aggregates can be effectively distinguished from each other. Particularly from day 2 to day 6, the nonlinearity parameter of aggregate #2 has an average value of two times the nonlinearity parameter of aggregate #3. It can also be observed from Fig. 10 that aggregate #3 has a higher nonlinearity parameter than aggregate #4 by day 3 and there is a clear distinction between the nonlinearity parameter for aggregates #3 and #4 by day 4. This relatively early differentiation of aggregate reactivity (i.e., between moderately reactive, marginally reactivity and non-reactive aggregates) is one potential advantage of the developed NIRAS method. Further research is necessary to validate these results using aggregates with a wide range of reactivity.

Together, these results highlight two key needs in terms of improving tests for aggregate screening: (1) tests are needed which are able to discriminate between aggregates of similar reactivity (e.g., moderately reactive versus marginally reactive) and (2) tests are needed which can distinguish aggregate reactivity relatively rapidly (i.e., within short exposure durations).

3.4. Microscopy

From a previously reported [37] petrographic analysis for mortar samples containing aggregate #1, both ASR gel and microcracking

were observed with this aggregate at early ages of exposure. The ASR gel was observed as early as after 2 days of exposure, and microcracks appeared from 4 days of exposure and then were seen gradually to open or widen with time. These events are somewhat consistent with the time when the nonlinearity parameter increases and decreases (Fig. 10). (These relationships between observed microstructural changes and measured nonlinearity parameter will be considered in further detail in Section 3.5.).

Mortar samples containing aggregate #2 were also examined petrographically. As shown in Fig. 11b and c, microcracks are not visible until day 6 at this magnification. The formation of microcracks in aggregate #2 thus occurs at a later age compared to aggregate #1, as expected due to the slower rate of reaction and lower overall reactivity of aggregate #2 according to expansion measurements and NIRAS results. After day 6, microcracks that propagate through aggregates and paste are seen to increase in width and become more open (Fig. 11d, e and f). As with aggregate #1, the increasing width of microcracks in the aggregate #2 mortar apparently coincides with the post-peak decrease of the nonlinearity parameter (Fig. 10).

For aggregate #2, it is also observed that an aggregate particle (in a region of interest at center-left of the images) disintegrates and grows more porous with increasing exposure periods. Based upon appearance, this is a likely a weathered chert. The damage within the aggregate is observed to start at day 6 of exposure and by day 8 a significant portion of the aggregate is observed to disintegrate. The exposure period when the disintegration of the aggregate is observed (day 6) in the images also coincides with the period when the nonlinearity parameter starts to decrease after the initial increase.

3.5. Physical interpretation of NIRAS results

The NIRAS technique has been shown to distinguish ASR-damaged samples from undamaged samples and to distinguish among aggregates of varying alkali–silica reactivity. The measured nonlinearity parameter was observed to increase with increasing damage due to ASR. But, as seen in Fig. 10, the nonlinearity parameters of aggregates #1 and #2 do not monotonically increase with exposure, which is inconsistent with the increasing expansion measured over time for these aggregates (Fig. 7). Thus, it is imperative to inter-relate the variation of the nonlinearity parameter with the changes occurring in the specimen during progressive ASR. The pattern of the changing nonlinearity parameter for the two more reactive aggregates #1 and #2 and the results obtained from microscopy will be used to relate the nonlinearity results with the observations of physical changes occurring in the microstructure.

The nonlinearity parameter of aggregate #1 reaches its peak by 4 days of exposure and decreases gradually afterwards, while the nonlinearity parameter of aggregate #2 has a slower progression, reaching the maximum value by 6 days of exposure, and decreasing and apparently stabilizing at low value by 10 days of exposure. In fact, the initial increase and eventual decrease of a different, complementary nonlinearity parameter (cubic coefficient β) of the same aggregate

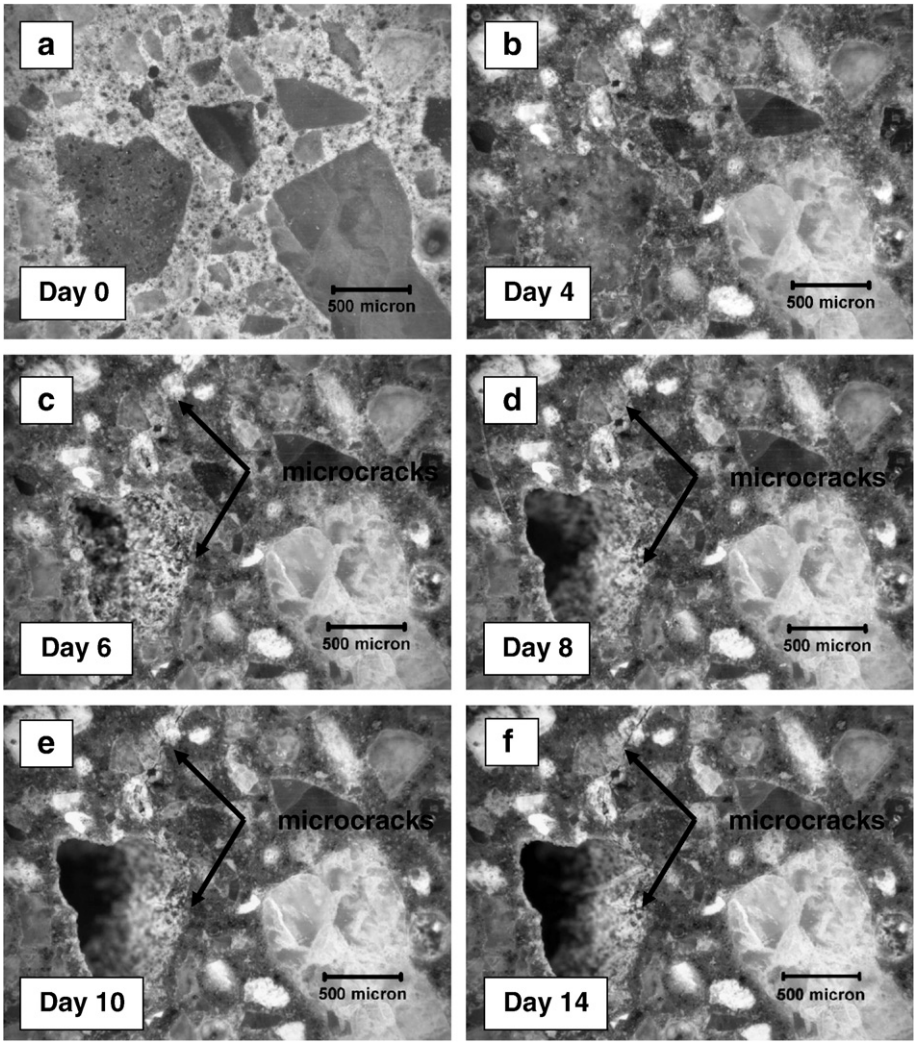

Fig. 11. Petrographic images of mortar bars with aggregate #2 (moderately reactive) at different exposure ages.

#1 were observed in previous research by the current authors, when using a different nonlinear technique based upon wave modulation [37]. In that study, a petrographic analysis performed on the mortar throughout the exposure period revealed ASR gel formation and subsequent debonding at the aggregate–paste interface, as well as cracking in the paste. It was suggested that these ASR-induced changes in the microstructure may be responsible for the initial increase and eventual decrease of the nonlinearity parameter.

Again, the change of material microstructure at different stages of ASR development may also contribute to the increase-then-decrease of the hysteresis parameter observed by the NIRAS technique in Fig. 10. Recall that researchers have established that the ASR gel product has unique elastic properties which differ from those of the aggregates and paste [19]. It may be proposed that as the amount of the ASR gel formed increases, it contributes to an increase in the overall heterogeneity of the mortar, resulting in an increase in the measured nonlinearity parameter. In addition, it has been found that the nonlinearity is closely related with the closing/opening of microcracks; the nonlinearity of microcracks is highest when the faces of a given microcrack are almost closed [43], which corresponds to initiation of microcracks. With expansion of ASR gel, new microcracks develop and grow in the paste and aggregate and interfacial debonding increases. Thus, the formation of microcracks during ASR could also contribute to the increase of nonlinearity parameter.

The cause of the relative post-peak decrease in nonlinearity parameter is not fully understood, but is likely the result of modifications to the material structure and properties. Two potential explanations for these measurements are presented from the perspective of gel formation and microcrack growth, respectively. First, the formation of crystalline products within the ASR gel due to interactions with calcium ions or carbonation, which could cause an overall stiffening effect, could cause the decrease of material nonlinearity. In addition, with continued soaking in high-temperature alkaline solutions, the ASR gel — which may be responsible for a large portion of the measured nonlinearity — becomes more fluid-like and/or may be largely lost to the surrounding solution, diminishing its influence on the measured nonlinearity. With respect to crack growth, previous research has found that the material nonlinearity becomes smaller when microcracks are open or not tightly closed [43]. Here, the continued formation and expansion of ASR gel can lead to widening of microcracks and coalescence into larger cracks. Crack widening in mortar bars undergoing progressive ASR was observed previously [37] and is apparent in the current research, as presented in Section 3.4.

It should be recognized, however, that ASR in cement-based materials is a complex process resulting in physical, chemical, and mechanical changes to the affected material. Such changes can have different and interactive effects on the measured acoustic nonlinearity, and it may be that the spatial variations in the microstructure (i.e., ASR-induced damage in the paste versus aggregate) may influence the measured nonlinearity parameter. For example, Ben Haha et al. [14] found that the cracks developed within aggregates can slow down the rate of expansion in laboratory samples; this decline in reaction rate could affect the measured nonlinearity measurements as well. However, cracking within the aggregate particles was not commonly observed in these mortars, perhaps due to the lack of restraint afforded by the current petrographic setup, and thus a definitive relationship between the location of the cracking and the measured nonlinearity parameter is not possible at this time. An apparent temporal correlation was found between the loss or apparent increased porosity (and presumable decreased modulus and strength) of highly reactive aggregate particles (Fig. 11) and a decrease in the nonlinearity parameter.

Thus, from the previous discussions, it is believed that the increase in the nonlinearity parameter is strongly dependent on the initial formation of gel and microcracks. With the progress of ASR, the initially formed cracks widen, and the gel grown more fluid-like

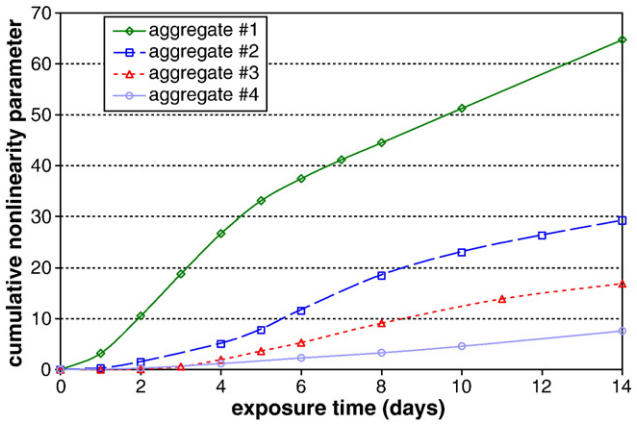

Fig. 12. Variation of cumulative nonlinear parameter with increasing exposure period.

(under AMBT conditions) resulting in a lesser contribution (or even a reverse effect) on the nonlinearity parameter. This would result in a decrease of the nonlinearity parameter once the rate of reaction slows, as observed in Fig. 10. In such a scenario the nonlinearity parameter that is measured at each testing instance would correspond to the newly formed gel and microcracks (or growth rate). Hence, a cumulative value (i.e., area under the nonlinearity parameter versus exposure time graph) would approximately represent the total extent of gel and microcrack formation or a more generally-defined ASR damage state.

The variation of the cumulative nonlinearity parameter with increasing exposure duration is plotted in Fig. 12. The cumulative nonlinearity parameters show very good correlations with measured AMBT expansions for all four aggregates, as shown in Fig. 13. Also, it can be clearly seen from Fig. 12 that the aggregates are distinguishable from each other as early as day 6 which was not evident in the expansion measurements (Fig. 7). Thus, such a cumulative nonlinearity parameter can be used to differentiate aggregates of varying alkali silica reactivity in a much shorter testing duration, compared to the expansion measurements. Importantly, this cumulative nonlinearity parameter could be used to define prescriptive limits on the value of nonlinearity parameter for classifying aggregates of varying reactivity. However, further testing with a wide range of aggregates is required before these limits can be defined.

4. Conclusions

A new nonlinear acoustic technique — Nonlinear Impact Resonance Acoustic Spectroscopy (NIRAS) — was developed and used to characterize the alkali-reactivity of different aggregates. Standard

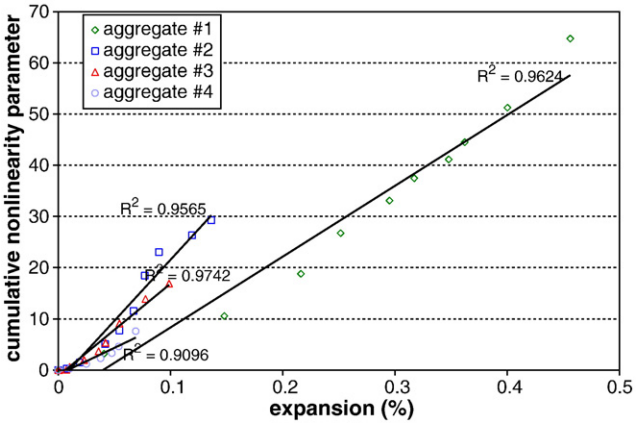

Fig. 13. Correlation between cumulative nonlinearity parameters and AMBT expansion.

mortar bars were cast and flexural resonance frequencies were experimentally obtained. The observed downward shift of resonance frequency with an increased excitation level was attributed to the nonlinearity in the mortar bar samples. The slope of the linear relationship in the plot of resonance frequency shift versus excitation magnitude was used to represent the state of ASR damage in mortar samples. It was shown that NIRAS is capable of distinguishing ASR damage in these samples and is more sensitive to ASR damage compared to the conventional linear vibration method. Furthermore, NIRAS can also differentiate aggregates with different levels of reactivity particularly in the early stages of ASR, which is a significant advantage over the standard expansion measurement tests used extensively in the industry. The varying pattern of nonlinearity parameters defined in NIRAS — measured for the two more reactive aggregates in this research — reflected the changes in the microstructure of materials, and were supported with the results from petrographic analysis. The cumulative value of the measured nonlinearity parameters correlated well with the AMBT expansion measurements and NIRAS thus is a promising technique for the evaluation of potential reactivity of aggregates and aggregate/paste combinations in laboratory tests. These findings also indicate that the proposed NIRAS technique is an effective nondestructive testing tool to detect and evaluate microstructural changes caused by ASR damage and could potentially be used to assess damage states in concrete structures. Further research is needed to consider a more broad range of aggregates, particularly to develop an improved understanding of the correlation between the influence of the ASR damage progression and the change of material nonlinearity.

Acknowledgements

The authors gratefully acknowledge support for this research from the Georgia Department of Transportation grant (GDOT 06-12) and Portland Cement Association Foundation Fellowship (PCA Fellowship 07-08). The contents of this material reflect the views of the authors, who are responsible for the facts and accuracy of the data presented. The contents do not necessarily reflect the views of the Portland Cement Association or Georgia Department of Transportation. The insights provided by Myron Banks, Jerry German, Mandi Reinshagen, Loren Petruny and Georgene Geary at GDOT, and Paul Tennis at PCA are appreciated. We also thank Robert Moser for help on the calibration of the compression test equipment.

References

[1] L.S. Dent Glasser, N. Kataoka, On the role of calcium in the alkali–aggregate reaction, Cem. Concr. Res. 11 (1981) 321–331.
[2] S. Chatterji, Chemistry of alkali–silica reaction and testing of aggregates, Cem. Concr. Comp. 27 (2005) 788–795.
[3] K.E. Kurtis, P.J.M. Monteiro, J.T. Brown, W. Meyer-Ilse, Imaging of ASR gel by soft X-ray microscopy, Cem. Concr. Res. 28 (1998) 411–421.
[4] R.N. Swamy, The alkali–silica reaction in concrete, Blackie, Glasgow, 1992.
[5] R. Helmuth, Alkali–silica reactivity: an overview of research, SHRP-C-342, National Research Council, Washington, DC, 1993.
[6] J.A. Farny, S.H. Kosmatka, Diagnosis and control of alkali–aggregate reactions in concrete, IS 413, Portland Cement Association, 1997.
[7] K.J. Folliard, B. Fourier, M. Thomas, ASR testing and evaluation protocols, protocol A: determining the reactivity of concrete aggregates and selecting appropriate measures for preventing deleterious expansion in concrete, Federal Highways Administration, Washington D.C, 2008.
[8] ASTM C 1260-07, Standard test method for determining the potential alkali reactivity aggregates (accelerated mortar-bar method). Annual book of ASTM standards vol. 04.02, (concrete and aggregates), Philadelphia (PA), 2007.
[9] AASHTO T 303-00. Standard method of test for accelerated detection of potentially deleterious expansion of mortar bars due to alkali–silica reaction. Standard specifications for transportation materials and methods of sampling and testing part 2B: tests, American Association of State Highway and Transportation Officials, Washington D.C., 2006.
[10] ASTM C 1293-08, Standard test method for concrete aggregates by determination of length change of concrete due to alkali–silica reaction. Annual book of ASTM standards, vol. 04.02 (concrete and aggregates), Philadelphia (PA), 2008.
[11] M. Thomas, B. Fournier, K. Folliard, J. Ideker, M. Shehata, Test methods for evaluating preventive measures for controlling expansion due to alkali–silica reaction in concrete, Cem. Concr. Res. 36 (2006) 1842–1856.
[12] ASTM Committee C09, Standard guide for petrographic examination of aggregates for concrete, ASTM C 295-03, Annual book of ASTM standards, West Conshohocken, PA.
[13] K.J. Folliard, M. Thomas, K.E. Kurtis, Guidelines for the use of lithium to mitigate or prevent ASR, FHWA-RD-03-047, Federal Highways Administration, National Research Council, Washington D.C, 2003.
[14] M. Ben Haha, E. Gallucci, A. Guidoum, K.L. Scrivener, Relation of expansion due to alkali silica reaction to the degree of reaction measured by SEM image analysis, Cem. Concr. Res. 37 (2007) 1206–1214.
[15] A. Shayan, A. Xu, H. Morris, Comparative study of the concrete prism test (CPT 60 °C, 100%RH) and other accelerated tests, Proceedings of the 13th ICAAR, Trondheim, Norway, 2008.
[16] M. DeGrosbois, E. Fontaine, Performance of 60 °C-accelerated concrete prism test for the evaluation of potential alkali-reactivity of concrete aggregates, Proceedings of the 11th ICAAR, Québec, Canada, 2000, pp. 277–286.
[17] D.Y. Lu, B. Fournier, P.E. Grattan-Bellew, Evaluation of accelerated test methods for determining alkali–silica reactivity of concrete aggregates, Cem. Concr. Comp. 28 (2006) 546–554.
[18] J.H. Ideker, B.L. East, K.J. Folliard, M. Thomas, B. Fournier, The current state of the accelerated concrete prism test, Proceedings of the 13th ICAAR, Trondheim, Norway, 2008.
[19] J.W. Phair, S.N. Tkachev, M.H. Manghnani, R.A. Livingston, Elastic and structural properties of alkaline–calcium silica hydrogels, J. Mater. Res. 20 (1995) 344–349.
[20] G. Giaccio, R. Zerbino, J.M. Ponce, O.R. Batic, Mechanical behavior of concretes damaged by alkali–silica reaction, Cem. Concr. Res. 38 (2008) 993–1004.
[21] A.E.K. Jones, L.A. Clark, The effects of ASR on the properties of concrete and the implications for assessment, Engr. Struct. 20 (9) (1998) 785–791.
[22] R.N. Swamy, M.M. Al-Asali, Engineering properties of concrete affected by alkali–silica reaction, ACI Mater. J. 85 (1988) 367–374.
[23] S. Amasaki, N. Takagi, The estimate for deterioration due to alkali–silica reaction by ultrasonic spectroscopy, Proceedings of the 8th ICAAR, Kyoto, Japan, 1989, pp. 839–844.
[24] J. Bungey, Ultrasonic testing to identify alkali–silica reaction in concrete, Br. J. Non-Destr. Test. 33 (1991) 227–231.
[25] K. Saint-Pierre, P. Rivard, G. Ballivy, Measurement of alkali–silica reaction progression by ultrasonic waves attenuation, Cem. Concr. Res. 37 (2007) 948–956.
[26] Pier Paolo Delsanto, Universality of nonclassical nonlinearity: application to nondestructive evaluations and ultrasonics, Springer, 2006.
[27] K. Van Den Abeele, J. De Visscher, Damage assessment in reinforced concrete using spectral and temporal nonlinear vibration techniques, Cem. Concr. Res. 30 (9) (2000) 1453–1464.
[28] J.-Y. Kim, L.J. Jacobs, J. Qu, J.W. Littles, Experimental characterization of fatigue damage in a nickel-base superalloy using nonlinear ultrasonic waves, J. Acoust. Soc. Am. 120 (3) (2006) 1266–1273.
[29] J. Herrmann, J.-Y. Kim, J. Qu, L.J. Jacobs, Assessment of material damage in a nickel-base superalloy using nonlinear Rayleigh surface wave, J. Appl. Phys. 99 (2006) 124913.
[30] C. Pruell, J.-Y. Kim, J. Qu, L.J. Jacobs, Evaluation of plasticity-driven material damage using Lamb waves, Appl. Phys. Lett. 91 (23) (2007) 231911.
[31] M. Kögl, S. Hurlebaus, L. Gaul, Finite element simulation of non-destructive damage detection with higher harmonics, NDT E Int. 37 (2004) 195–205.
[32] D. Donskoy, A. Sutin, A. Ekimov, Nonlinear acoustic interaction on contact interfaces and its use for nondestructive testing, NDT E Int. 34 (4) (2001) 231–238.
[33] A.E. Ekimov, I.N. Didenkulov, V.V. Kazakov, Modulation of torsional waves in a rod with a crack, J. Acoust. Soc. Am. 106 (3) (1999) 1289–1292.
[34] K. Warnemuende, H.-C. Wu, Actively modulated acoustic nondestructive evaluation of concrete, Cem. Concr. Res 34 (4) (2004) 563–570.
[35] C. Payan, V. Garnier, J. Moysan, P.A. Johnson, Applying nonlinear resonant ultrasound spectroscopy to improving thermal damage assessment in concrete, JASA Express Lett. 121 (4) (2007) 125–130.
[36] X.J. Chen, J.-Y. Kim, K.E. Kurtis, J. Qu, C.W. Shen, L.J. Jacobs, Characterization of progressive microcracking in Portland cement mortar using nonlinear ultrasonics, NDT E Int. 41 (2008) 112–118.
[37] J. Chen, A.R. Jayapalan, K.E. Kurtis, J.-Y. Kim, L.J. Jacobs, Nonlinear wave modulation spectroscopy method for ultra-accelerated ASR assessment, ACI Mater. J. 106 (2009) 340–348.
[38] P.A. Johnson, B. Zinszner, P.N.J. Rasolofosaon, Resonance and elastic nonlinear phenomena in rock, J. Geophy. Res. 101 (B5) (1996) 11553–11564.
[39] K.R. McCall, R.A. Guyer, Equation of states and wave propagation in hysteretic nonlinear elastic materials, J. Geophy. Res. 99 (B12) (1994) 23887–23897.
[40] L.D. Landau, E.M. Lifshitz, Theory of elasticity, (3 rd Edition)Pergamon Press, London, 1986.
[41] A. Migliori, J.L. Sarrao, Resonant ultrasound spectroscopy, Wiley, New York, 1997.
[42] K. Van Den Abeele, Multi-mode nonlinear resonance ultrasound spectroscopy for defect imaging: An analytical approach for the one-dimensional case, J. Acoust. Soc. Am. 122 (2007) 73–90.
[43] J.-Y. Kim, J.-S. Lee, A micromechanical model for nonlinear acoustic properties of interfaces between solids, J. Appl. Phys. 101 (2007) 043501.